



UNIVERSITY OF LEEDS

This is a repository copy of *Stretch Rate Effects and Flame Surface Densities in Premixed Turbulent Combustion up to 1.25 MPa*.

White Rose Research Online URL for this paper:
<http://eprints.whiterose.ac.uk/89075/>

Version: Accepted Version

Article:

Bagdanavicius, A, Bowen, PJ, Bradley, D et al. (2 more authors) (2015) Stretch Rate Effects and Flame Surface Densities in Premixed Turbulent Combustion up to 1.25 MPa. *Combustion and Flame*, 162 (11). 4158 - 4166. ISSN 0010-2180

<https://doi.org/10.1016/j.combustflame.2015.08.007>

© 2015, The Combustion Institute. Published by Elsevier Inc. Licensed under the Creative Commons Attribution-NonCommercial-NoDerivatives 4.0 International
<http://creativecommons.org/licenses/by-nc-nd/4.0/>

Reuse

Unless indicated otherwise, fulltext items are protected by copyright with all rights reserved. The copyright exception in section 29 of the Copyright, Designs and Patents Act 1988 allows the making of a single copy solely for the purpose of non-commercial research or private study within the limits of fair dealing. The publisher or other rights-holder may allow further reproduction and re-use of this version - refer to the White Rose Research Online record for this item. Where records identify the publisher as the copyright holder, users can verify any specific terms of use on the publisher's website.

Takedown

If you consider content in White Rose Research Online to be in breach of UK law, please notify us by emailing eprints@whiterose.ac.uk including the URL of the record and the reason for the withdrawal request.



eprints@whiterose.ac.uk
<https://eprints.whiterose.ac.uk/>

Stretch Rate Effects and Flame Surface Densities in Premixed Turbulent Combustion up to 1.25 MPa

A. Bagdanavicius^a, P. J. Bowen^b, D. Bradley^{c*}, M. Lawes^c, M.orkous S. Mansour^{d,e}

^a Department of Engineering, University of Leicester, Leicester LE1 7RH, UK

^b Cardiff School of Engineering, Cardiff University, Cardiff CF24 3AA

^c School of Mechanical Engineering, University of Leeds, Leeds LS2 9JT, UK

^d Clean Combustion Research Center, King Abdullah University of Science and Technology, Thuwal, Saudi Arabia

^e Department of Mechanical Engineering, Helwan University, Cairo, Egypt

* Corresponding Author E-mail address: d.bradley@leeds.ac.uk

Key words

Turbulent premixed flame, burning velocity, flame stretch rate, flame surface density, Markstein number.

Abstract

Independent research at two centres using a burner and an explosion bomb has revealed important aspects of turbulent premixed flame structure. Measurements at pressures and temperatures up to 1.25 MPa and 673 K in the two rigs were aimed at quantifying the influences of flame stretch rate and strain rate Markstein number, Ma_{sr} , on both turbulent burning velocity and flame surface density. That on burning velocity is expressed through the stretch rate factor, I_0 , or probability of burning, $P_b^{0.5}$. These depend on Ma_{sr} , but they grow in importance as the Karlovitz stretch factor, K , increases, and are evaluated from the associated burning velocity data. Planar laser tomography was employed to identify contours of reaction progress variable in both rigs. These enabled both an appropriate flame front for the measurement of the turbulent burning velocity to be identified, and flame surface densities, with the associated factors, to be evaluated. In the explosion measurements, these parameters were derived also from the flame surface area, the derived $P_b^{0.5}$ factor and the measured turbulent burning velocities. In the burner measurement they were calculated directly from the flame surface density, which was derived from the flame contours.

A new overall correlation is derived for the $P_b^{0.5}$ factor, in terms of Ma_{sr} at different K and this is discussed in the light of previous theoretical studies. The wrinkled flame surface area normalised by the area associated with the turbulent burning velocity measurement, and the ratio of turbulent to laminar burning velocity, u_t/u_l , are also evaluated. The higher the value of $P_b^{0.5}$, the more effective is an increased flame wrinkling in increasing u_t/u_l . A correlation of the product of k and the laminar flame thickness with Karlovitz stretch factor and Markstein number is explored using the present data and those of other workers. Some generality is revealed, enabling the wave length associated with the spatial change in mean reaction progress variable to be expressed by the number of laminar flame thicknesses, and the flame volume to be found.

1. Introduction

Although the influence of flame stretch rate on the unstretched laminar burning velocity, is reasonably well quantified through the product of the laminar Karlovitz stretch factor and appropriate Markstein number, there is no directly comparable quantitative understanding of the influence of turbulent stretching of the flame on the turbulent burning velocity, u_t .

The importance of thermo-diffusive influences was shown experimentally through the influence of Lewis number at increasing Karlovitz stretch factor on the normalised turbulent burning velocity by Abdel-Gayed et al. [1]. Asymptotic analysis attributed the changes to thermo-diffusive effects and possible flame extinctions at high flame stretch rates. The influence of the latter also featured in quantifications of a probability of burning, P_b [2,3]. These approaches expressed the influences of the distribution of strain rates in the flow and the flame extinction stretch rate on the computed volumetric heat release rate in laminar flamelet modelling. Later it also embraced thermo-diffusive influences through the Markstein length, prior to any extinction [4].

Flamelet modelling involving flame surface density, Σ , initially emphasised the role of thermo-diffusive and stretch rate influences, rather than flamelet extinctions, on the deviation of effective laminar burning velocity from that of the unstretched laminar burning velocity, u_l . The overall mass rate of turbulent burning was expressed by the product of a mean surface area, a , of the appropriate turbulent flame front, the turbulent burning velocity, u_t , and the density, ρ_u , of the initial mixture. This was equated to the volumetric mass rate of burning at the wrinkled flame surface, with Σ integrated over the entire volume, V , of the reacting flame brush, giving:

$$u_t a \rho_u = \rho_u \int_V \Sigma I_o u_l dv. \quad (1)$$

Here, I_o is a factor that allows for the influence of the stretch rate in changing the effective laminar burning velocity. Bray [5] derived an expression for the dependency of I_o upon the laminar Karlovitz stretch factor and Markstein number. The probability of burning was related in [6] to the turbulent burning velocity that would exist in the absence of stretch rate effects, u_{t0} , by:

$$u_t/u_{t0} = P_b^{0.5}. \quad (2)$$

It follows from Eqs. (1) and (2) that:

$$u_t a \rho_u = \rho_u \int_V \Sigma P_b^{0.5} u_l dv = \rho_u u_l P_b^{0.5} A, \text{ and } P_b^{0.5} = I_o, \quad (3)$$

where $A = \int_V \Sigma dv$, is the total flame surface area throughout the flame brush.

Measurements in lean premixed CH_4/air flames on a low swirl burner by Shepherd and Cheng [7] confirmed the balance of the two mass burning rate expressions in Eq. (3). Markstein numbers were close to zero, and I_o close to unity. They were of the view that the flame surface measurements were the more simple to perform and these should be used to

check theoretical models. More recently, with similar mixtures and equivalence ratios, ϕ , between 0.7 and 1.0, Meng Zhang et al. [8] have also, found values of I_0 close to unity from estimated 3D flame surface density measurements.

The direct numerical simulations, DNS, of Hawkes and Chen [9] and Dunstan et al. [10], for unity and near-unity Lewis numbers, also showed values of I_0 close to unity, with no strong geometric dependence throughout the flame brush, and only a weak dependence on turbulent velocity. This is consistent with the regime envisaged by Damköhler, in which the increase in u_t due to turbulence was predominantly attributed to increase in flame surface area [11].

However, just as laminar flames are affected by non-unity Lewis numbers and non-zero Markstein numbers, turbulent flames also are affected by thermo-diffusive effects [12]. Theoretical values of $P_b^{0.5}$ have been computed in [13] over a wide range of values of the strain rate Markstein number, Ma_{sr} , and Karlovitz stretch factor, K . Allowances were made for flame instabilities at the lower values of K and flame extinctions at the higher values. Furthermore, both experimentally and theoretically, limitations arise because of the difficulty of allowing for the transient effects associated with rapidly changing turbulent fluctuations [14] and their effect on the values of $P_b^{0.5}$. For example, the DNS of Chen and Im [15], showed that as the turbulence increases, the flame propagation becomes less responsive to unsteady straining and the effective values of Ma_{sr} decrease. Experimentally, it has been shown that transient flame stretch rate excursions in excess of the steady state value for flame extinction do not necessarily lead to extinction [16]. Such transient effects limited the accuracy of the predictions of $P_b^{0.5}$ in [13].

The present study was undertaken to remedy the dearth of experimental data on $P_b^{0.5}$ for non-zero laminar Markstein numbers, over wide ranges of flame conditions and values of the Karlovitz stretch factor. The derived values of $P_b^{0.5}$ are based upon Eq. (3), with measurements of u_t and of flame surface densities derived from spatial contours of the mean reaction progress variable, \bar{c} . Measurements were made on different types of flame: explosion flames in a fan-stirred bomb at the University of Leeds, and burner flames in the high pressure burner at Cardiff University. Theoretical calculations were made in the course of the study of $P_b^{0.5}$ at different K for a datum Markstein number of zero.

The measured flame surface density is related to the mean reaction progress variable, \bar{c} , by:

$$\Sigma = k\bar{c}(1 - \bar{c}), \quad (4)$$

where k is the reciprocal of a wave length that expresses the spatial change in \bar{c} . Values of k were found over the wide range of investigated conditions. Combined with those from other sources, these are able to give an improved understanding of turbulent flame structure.

2. Stretched Flame Analyses

2.1 Probability of Burning and the Turbulent Burning Velocity

Early generalisations of measured values of u_t/u_l were expressed first in terms of the product of Karlovitz and Lewis number of the deficient reactant, KLe [3], then later, KMa_{sr} [6,13]. Latterly, it has proved necessary to separate K and Ma_{sr} [17-19]. This was particularly so in the low K regime of unstable flamelets, in which flame wrinkling due to laminar flame instabilities interacts with the onset of very mild turbulence at low values of the rms turbulent velocity, u' . The instabilities increase with increasingly negative values of Ma_{sr} . This is Regime A in Fig. 1, which is reproduced from [17], and shows $U = u_t/u'_k$ plotted against K for different Ma_{sr} . Here u'_k is the effective rms turbulent velocity to which the expanding flame kernel is exposed. It increases as the kernel is exposed to an increasing range of turbulent wave lengths [17,18]. Regime B is comprised of more stable flames, in which u_t increases with the increased flame wrinkling and associated flame surface area. Although the effective laminar burning velocity is influenced by the local stretch rate, appreciable localised flame extinctions are largely avoided. The flames in the present study are predominantly in this regime. Regime C, incompletely explored, is one of increasing partial flame extinctions and, ultimately of flame quenching at high K .

The value of K is equal to the rms strain rate, u'/λ , where λ is the Taylor scale of turbulence, multiplied by a chemical lifetime, δ/u_l . This can be regarded as a ratio of chemical to eddy lifetimes. Here δ is the laminar flame thickness given by the kinematic viscosity normalised by u_l . It is shown in [18] that:

$$K = 0.25(u'/u_l)^2 R_l^{-0.5}, \quad (5)$$

where R_l is the turbulent Reynolds number, based on u' and the integral length scale, l . In the present work, there was a greater isotropy in the bomb than that in the burner turbulence. For the latter, mean values of both length scale and u' were employed. There was no evidence of any incompatibility in the values of K found in this way from the two rigs.

The theoretical values presented in [6,13] show $P_b^{0.5}$ to be sensitive to changes in K and Ma_{sr} , but much less so to independent additional changes in R_l . This was confirmed experimentally,

in [6] and proportionality was established between U and $P_b^{0.5}$ for different Ma_{sr} at constant K . Because $P_b^{0.5}$ at a given K is dependent upon Ma_{sr} , it is convenient to express its value at a given K and Ma_{sr} by $(P_{bMa}^{0.5})_K$. If there are no instabilities or partial extinctions and the flame is un-stretched, this parameter has a value of unity. If it is stretched, the value is changed to an extent that depends upon Ma_{sr} . If K is constant, an increase in Ma_{sr} , with Ma_{sr} positive, decreases U and $P_b^{0.5}$, With Ma_{sr} negative these values increase. If Ma_{sr} is assigned a value of zero, all the conditions are fulfilled for the corresponding values of $(P_{bMa}^{0.5})_K$, now designated by $(P_{bo}^{0.5})_K$, to be close to unity, with minimal changes from this value.

This makes $(P_{bo}^{0.5})_K$ for the different values of K a suitable datum for the derivation of more general values of $(P_{bMa}^{0.5})_K$, from the corresponding values of U , indicated by $(U_{Ma})_K$. The proportionality between U and $(P_{bMa}^{0.5})_K$ for different Ma_{sr} at the same value of K is then expressed by:

$$\left(\frac{P_{bMa}^{0.5}}{P_{bo}^{0.5}} \right)_K = \left(\frac{U_{Ma}}{U_o} \right)_K. \quad (6)$$

Values of the datum $(P_{bo}^{0.5})_K$, allowing for flame stretch rate and localised extinctions, computed in [13] are shown by the broken curves in Fig. 2 to be close to unity. However, it is apparent from Figs. 5 and 6 of [13] that the computed values of U under-estimate the measured values by about 10% as K approaches unity. To correct for this, the datum values of $(P_{bo}^{0.5})_K$ were correspondingly increased to the values shown by the full line curve in Fig. 2.

Values of $(P_{bMa}^{0.5}/P_{bo}^{0.5})_K$, at different Ma_{sr} and K , were then found from both the measurements of $(U_{Ma}/U_o)_K$ in explosion flames [17,18] and in burner flames [20,21]. With the theoretical values of $P_{bo}^{0.5}$ given by the full line curve in Fig. 2, it was possible from Eq. (6) to express $P_{bMa}^{0.5}$ as a function of K for different Ma_{sr} .

2.2 Flame Surface Density and k .

Experimental evaluation of Σ entailed the use of thin planar optical sheets, within which seeded flame Mie images indicated the flame wrinkling. For both the spherical explosion and cylindrical burner flames, the spatial distribution of the contours of the mean reaction progress variable, \bar{c} , was obtained from these images using the expressions of Lipatnikov and Chomiak [12,22], respectively. From Eq. (4), the total overall flame area, A , is given by:

$$A = \int_V k\bar{c}(1 - \bar{c}) dv, \quad (7)$$

and, from Eq. (3),

$$(u_t/u_l) = (A/a)(Pb_{Ma}^{0.5})_K. \quad (8)$$

In the case of the explosion flames, the mean turbulent flame surface area, a for measuring the mass rate of burning is defined by $\bar{c} = 0.59$ (17,18) and hence a is known. With both burning velocities known, and $(Pb_{Ma}^{0.5})_K$ derived from Eq. (6) and Fig. 2, A could be found for known values of K and Ma_{sr} from Eq. (8). The spatial distribution of \bar{c} then enabled k to be evaluated from Eq. (7). In the case of the burner flames, Σ was derived from the two-dimensional optical measurements. Values of k could then be found from Eq. (4) for each value of \bar{c} , as described in [7].

3. Experimental Rigs and Methodology

The experimental pressures ranged up to 1.25 MPa and the temperatures up to 675K. Ranges of these for the two rigs, as well as of the fuels, equivalence ratios, and rms turbulent velocities, are given in Table 1. Reference sources for Ma_{sr} and u_l also are given. Experimental values of K ranged from 0.06 to 2.5, and of Ma_{sr} from -11 to 5.

3.1 High Pressure Burner Experiments

The horizontal burner, shown in Fig. 3, fired into an inner combustion chamber, enclosed within an optical pressure casing. The optically accessed combustion section was connected to a compressor and heat exchanger, allowing heated pressurised combustion air to be delivered at the required conditions. The inner combustion chamber, of 150 mm square section, had four internal quartz windows aligned with the outer casing, enabling extensive optical access to the combustion chamber. The fuel/air mixture was fed along a cylindrical tube into the combustion chamber. This was fitted with an annular methane diffusion flame pilot burner, to aid stability while adjusting the operating conditions. The pilot was switched off prior to taking measurements. The main burner was supplied with premixed fuels and air via a turbulence plate that generated uniform downstream turbulence. The fuel gas supply was connected to a mixing chamber upstream of this plate, along with the preheated combustion air, seeded with aluminium oxide particles for laser diagnostic measurements. The gaseous fuel, combustion air, and seed air were measured simultaneously using Coriolis flow meters. Temperatures and pressures remained reasonably steady, with fluctuations not exceeding 5% of the target values.

Two laser-based measurement techniques were employed. Two-dimensional laser Doppler velocimetry was employed to measure the velocity profile and turbulence characteristics at

the burner exit under the elevated ambient conditions [20]. The integral length scale of the turbulence varied from 7 to 15 mm at 0.3 MPa and from 2 to 8 mm at 0.7 MPa. Planar laser tomography quantified the turbulent flame characteristics. This technique was based on the density of the products being lower than that of the reactants. Consequently, upon reaction, the seed density decreased and the scattered light intensity fell. As the flame thickness is small, a clear demarcation was generated between products and reactants, which can be identified as the flame front. Images of the flame front were recorded using a Photron APX-rs high speed camera, mounted perpendicularly, and synchronised with a pulsed (Nd:YAG) sheet laser. For each experimental condition 1000 images were recorded. Each individual image was carefully filtered using morphological image processing techniques, compensated for background noise, and ultimately converted from greyscale to binary images.

Measurements of flame brush thickness and flame surface densities characteristics followed the methodology of Lachaux et al. [27]. The latter were obtained as a function of \bar{c} , derived from their contours, as described in [27], by Shepherd and Cheng [7]. A progress variable contour map was first obtained with \bar{c} ranging from 0.05 to 0.95 at intervals of 0.1, and the areas found between the adjacent isolines of \bar{c} . The instantaneous flame front contours were superimposed on the \bar{c} contour map and the length of the flame contour line falling within the area of interest was calculated. This culminated in the mapping of the two dimensional flame surface density.

The flame front area was found using the "statistical" method, whereby the flame front area was calculated using each individual binary flame image first. Then the average flame front area for each test was found using the statistical analysis. Subsequent comparisons showed the burner flame front location to be consistently close to $\bar{c} = 0.5$, which defines the surface area appropriate to the mass burning rate on burners [18]. More details of the image processing are available in [21]. Values of k were found between $\bar{c} = 0.2$ and 0.8, over which range they remained fairly constant. Typical flame images are shown in Fig. 4. Turbulence velocities did not exceed 2.67 m/s, and there was little small scale wrinkling.

3.2 Fan-stirred Bomb Experiments

The spherical stainless steel, fan-stirred, bomb, shown in Fig. 5, has three pairs of orthogonal windows of 150 mm diameter and has been described in [17,18]. The four fans, arranged in a tetrahedron formation, were rotated by electric motors with independent speed control. The internal diameter is 380 mm and the maximum operational initial pressure was 1.5 MPa. The gaseous mixture was heated to 358K by a 3 kW electric heater, located at the wall. Initial gas temperature was measured with a sheathed chromel-alumel thermocouple. Four fans, each

driven by an 8 kW electric motor, were located close to the wall of the bomb. They initially mixed the reactants and, at higher fan speeds, of up to 10,000 rpm, generated the turbulence. The rms turbulent velocity increased linearly with the synchronized speed of the fans, and the integral length scale of 20 mm was independent of fan speed and initial pressure. Both were measured by laser Doppler velocimetry.

Liquid fuel was injected with a gas tight syringe, through a needle valve, and gaseous fuel was supplied directly. Pressures were measured by a Kistler pressure transducer. A central spark plug with ignition energies of about 23 mJ, was supplied from a 12 V transistorised automotive ignition coil. Further details are given in [18].

Flame images were captured, by schlieren cine photography, to obtain flame speeds, recorded with a high speed Phantom digital camera, at up to 9,000 frames/s. Five explosions were performed and complete data sets obtained for each separate condition. For each explosion the mean flame radii, obtained from measurements of the projected flame area, were plotted against time. Simultaneous with schlieren photography, measurements of Mie-scattered light from a thin planar sheet differentiated between unburned and burned gas, in a similar manner to that for the burner experiments. These were obtained with a copper vapour laser from particles of less than a micron diameter. The images were recorded, at 4,500 frames/s, in synchronisation with the schlieren camera. Values of \bar{c} were found from the images [28].

4. Experimental Results

4.1 Values of $P_b^{0.5}$

Only the most negative values of Ma_{sr} might be expected to be within the laminar/turbulent instability Regime A. Similarly, the present flame surface data are confined to Regime B. Because the new experimental data produced no significant changes to those involving U , K and Ma_{sr} in Fig. 1, the correlation law for U , developed in [17] for outside the unstable regime, continued to be employed, in the form:

$$u_t/u'_k = U = \alpha K^\beta. \quad (9)$$

For positive values of Ma_{sr} , up to 5,

$$\alpha = 0.023(30 - Ma_{sr}) \text{ and } \beta = 0.0103(Ma_{sr} - 30). \quad (10)$$

For $Ma_{sr} = 0$ and U_o

$$\alpha = 0.8 \text{ and } \beta = -0.239. \quad (11)$$

For negative values of Ma_{sr} , up to -23,

$$\alpha = 0.09(7 - \text{Ma}_{\text{sr}}) \text{ and } \beta = -0.008(\text{Ma}_{\text{sr}} + 30). \quad (12)$$

Experimentally based values of $(P_{b\text{Ma}}^{0.5}/P_{bo}^{0.5})_K$, obtained from Eq. (6), are shown in Figs. 6 and 7. These are plotted against K for different Ma_{sr} and calculated from individual experimental data points for U . Also shown are best-fit curves based on polynomial functions, not based on any a priori considerations. There are no burner data for Ma_{sr} more negative than -3.8, and the most negative value for the bomb is -11. Positive values extend to 5. The scattered points are due to the random behaviour of such flames and the scatter is similar for both rigs.

The theoretical datum values of $(P_{bo}^{0.5})_K$ are given by the full line curve in Fig. 2 for $\text{Ma}_{\text{sr}} = 0$. These were used to derive the values of $P_{b\text{Ma}}^{0.5}$ from those of $P_{b\text{Ma}}^{0.5}/P_{bo}^{0.5}$ in Figs. 6 and 7. Some typical values of $P_{b\text{Ma}}^{0.5}$ for different Ma_{sr} are shown in Fig. 8, derived in this way using the values of $(P_{bo}^{0.5})_K$, shown up to $K = 1.0$ in Fig. 2.

Finally, the best overall smoothed correlations of $(P_{b\text{Ma}}^{0.5})_K$, over the full range of Ma_{sr} are presented in the form of the full line curves in Fig. 9. These include the theoretical datum curve for $\text{Ma}_{\text{sr}} = 0$, with an extrapolation shown by the dashed curve to $K = 1.3$. Because of the more restricted ranges of $(P_{b\text{Ma}}^{0.5})_K$, than of U , it is more difficult to indicate the onset of the significant flame extinction Regime C of Fig. 1 on Fig. 9. An attempt to do this for the most positive Ma_{sr} values is made with the dotted curve for $\text{Ma}_{\text{sr}} = 5$ on Fig. 9, based on extrapolated values.

4.2 Values of k

The methods of derivation of k are described for both burner and bomb in Section 2. Two sets of k values for positive and negative Ma_{sr} , between +6 and -6 are plotted against K , in Fig. 10. Not surprisingly, there is appreciable scatter in these experimental points, but the best fit curves show some general differentiation between positive and negative values of Ma_{sr} , with somewhat greater values of k for negative Ma_{sr} . The logarithmic scale for K gives a better resolution close to the laminar/turbulent unstable Regime A, discussed in detail in [17]. For $\text{Ma}_{\text{sr}} = -11$, the boundary of this regime on Fig. 1 is at about $K = 0.04$. The present data are not applicable to Regime A of Fig. 1.

5. Discussion

The results from both rigs are compatible, with the stretch rate effects on turbulent burning velocity and $P_{b\text{Ma}}^{0.5}$ being similar. It is interesting that these basic combustion attributes seem to have little dependency on the detailed burner and bomb geometries. This aspect has also

been noted, in all but V-flames, in the DNS of [10]. The large range of fuel mixtures and operating conditions for burner and explosion bomb, apparent in Table 1, combined with the stochastic nature of turbulence, inevitably produce a large scatter in values of both U , and $(P_{bMa}^{0.5})_K$. Notwithstanding these factors, clear trends emerge from the best-fit curves and Figs. 1 and 9 show both U and $P_{bMa}^{0.5}$ to be a function of K and Ma_{sr} . The values of $(P_{bMa}^{0.5})_K$, plotted against K in Fig. 9, show, in particular, the consequences of the sign of Ma_{sr} on $(P_{bMa}^{0.5})_K$. A decrease in Ma_{sr} , which often occurs through an increase pressure, can lead to an increase in $(P_{bMa}^{0.5})_K$.

A useful inter-linking expression, involving Eqs. (5) and (8), that introduces u_t/u_l , is:

$$u_t/u_l = (u_t/u')(u'/u_l) = U(4K(u_l l/\nu)^{0.5})^{2/3} = (A/a)(P_{bMa}^{-0.5})_K. \quad (13)$$

Consequently, u_t/u_l and A/a can be found as a function of K , for different values of Ma_{sr} and $u_l l/\nu$. For fixed values of these two parameters, in Regime B, because K increases faster than U diminishes, an increase in the turbulence through an increase in K , increases both u_t/u_l and A/a . The influences of K and Ma_{sr} on $P_b^{0.5}$, u_t/u_l , A/a , as well as flame extinctions, are illustrated by the plots for $Ma_{sr} = 5$ and -5 in Figs 11(a) and (b), respectively, with $u_l l/\nu = 27.8$. The last is a typical value in engines ($u_l = 0.4$ m/s, $l = 2.6$ mm, $\nu = 1.345 \cdot 10^{-6}$ m²/s). Data are extrapolated beyond $K = 1.3$.

For both values of Ma_{sr} increases in u_t/u_l , and flame wrinkling, through A/a , are apparent. However, in Fig. 11(a), with positive Ma_{sr} , for increases in K beyond 0.6, $P_b^{0.5}$, begins to decrease, ever more sharply, with increasing localised flame extinctions. As long as the effects of increasing flame wrinkling predominate over those of increasing stretch rate, then, u_t/u_l increases. This balance is different in Fig. 11(b), with negative Ma_{sr} . Now increases in K initially enhance $P_b^{0.5}$, and less wrinkling is required to attain a given u_t/u_l . For example, these figures show that a value of u_t/u_l of 15 is attained with $A/a = 31.8$ for $Ma_{sr} = 5$, whereas this same value of u_t/u_l is attained with a lesser value of A/a , namely 12.4, for $Ma_{sr} = -5$. The respective values of $P_b^{0.5}$ are 0.49 and 1.2.

As local extinctions increase with increasing K , $P_b^{0.5}$ continues to fall, and u_t/u_l would be expected to pass through a maximum in Regime C, which is not entered in the present study. The flames become highly convoluted with increasing K and lose coherence, with wisps of flame appearing in dispersed regions of lower stretch rate, Eq. (3) becoming inapplicable, and the relationships upon which Fig 11 is based no longer valid. At $P_b^{0.5} \sim 0.1$ quenching becomes complete. Figure 1 and Figs. 11(a) and (b) suggest that the flames of Fig. 11(a)

approach quenching when K lies between 2 and 2.5, with $P_b^{0.5} \sim 0.1$, whereas those of Fig. 11(b), with a higher extinction stretch rate, have a value of $P_b^{0.5}$ of as high as about 0.75 in the middle of this range. Such is the degree of wrinkling with limit flames, their curvature stretch rate might well be dominant in the extinction mechanism in Regime C, indicated in Fig. 1 and partially by the “Quenching” curve in Fig. 9. The DNS of Chen and Im [30] show extinctions at large negative curvature.

Values for $Ma_{sr} < -6$ lie on the boundary of the laminar/turbulent unstable Regime A. The instabilities in Regime A that lead to higher values of U with increasingly negative Ma_{sr} are the result of additional wrinkling, beyond that due to laminar instabilities, and provided by the developing smallest turbulent wave lengths on the Gibson scale [17,31]. For $Ma_{sr} = 3$ the instabilities terminated when K reached 0.009 and for $Ma_{sr} = -19$ when K reached 0.07. This suggests that none of the k data in Fig. 10 fall within this regime, although the two best-fit curves for positive and negative Ma_{sr} suggest a slightly higher value of k for the latter.

An unsatisfactory aspect of the values of k plotted in Fig. 10 is that the wave length for the spatial change in \bar{c} , namely k^{-1} , is not combined with an appropriate length scale in a dimensionless grouping. The increased wrinkling at higher pressures in Regime A suggests that δ might be a relevant parameter for normalising the wave length, with $(k\delta)^{-1}$ representing the \bar{c} wave length in terms of laminar flame thicknesses. When k values in the unstable Regime A were normalised in this way, which was also employed in [32], the scatter with this normalisation was reduced, in comparison with that with k , as a result of the decrease in δ with increasing pressure [33]. This procedure was repeated with the present data, and also was applied to those from other researchers, and the results are presented in Fig.12. Much of the data suggest $(k\delta)^{-1} \sim 20$, but the burner values for $K < 0.3$ are often higher than this.

Multiplications of both sides of Eqs. (4) and (7) by δ create a flame volume density and an overall flame volume, $A\delta$. A near constancy of $k\delta$ in Regime B of Fig. 1 might be indicative of a maximum possible volumetric packing of the wrinkled flame surface, limited by the onset of localised flame extinctions at high curvatures.

6. Conclusions

1. Two diverse combustion rigs for studying controlled turbulent combustion, a burner and an explosion bomb, have shown similar effects of flame stretch rate on the turbulent burning velocities, over a wide range of fuels, pressures, and temperatures. The turbulent regime

studied extends from one that is just free of laminar/turbulent instabilities to one just prior to the onset of significant flame quenching.

2. The role of flame stretch rate in controlling the turbulent burning rate has been clearly demonstrated in terms of the Markstein number for strain rate and the Karlovitz stretch factor. The effects have been quantified through the derived $(P_{bMa}^{0.5})_K$ parameter. This increases as the Markstein number decreases and becomes negative.

3. For particular values of $(u_t l / \nu)$ and the derived values of $(P_{bMa}^{0.5})_K$, A/a and u_t/u_1 have been expressed as functions of K and Ma_{sr} . These showed the extent to which a more negative value of Ma_{sr} , and the associated higher the value of $P_{bMa}^{0.5}$, enable higher values of u_t/u_1 , to be achieved, and with less flame wrinkling. To attain a value of u_t/u_1 of 15 required one of A/a of 31.8, with $Ma_{sr} = 5$, but one of only 12.4 sufficed with $Ma_{sr} = -5$.

4. The findings demonstrate how mathematical modelling may be in error through the use of steady state values. Transient fluctuations change the effective Markstein numbers, and transient excursions to stretch rates in excess of the steady state flame extinction values may be tolerated without inducing flame extinctions.

5. Measurements included the derivation of contours of mean reaction progress variable and its reciprocal spatial wavelength, k . The data on k were combined with those of other researchers and multiplied by δ . Although there is much scatter in the plots against K , there is some indication at the higher values of K that $(k\delta)^{-1} \sim 20$.

6. Such an approximate possible limiting value is of interest in three contexts. It suggests a maximum possible volumetric packing of the wrinkled flame surface, limited by the possible onset of localised flame extinctions at high curvatures. It represents a spatial wave length for \bar{c} of 20 laminar flame thicknesses. It enables the flame volume density to be found and, along with the A/a data, the volume of the turbulent flame brush.

References

1. R.G. Abdel-Gayed, D. Bradley, M.N. Hamid, M. Lawes, Proc. Combust. Inst. 20 (1985) 505-512.
2. R.G. Abdel-Gayed, D. Bradley, A.K.C. Lau, Proc. Combust. Inst. 22 (1988) 731-738.
3. D. Bradley, A.K.C. Lau, M. Lawes, Phil. Trans. R. Soc. Lond. A338 (1992) 357-387.
4. D. Bradley, P.H. Gaskell, X.J. Gu, Proc. Combust. Inst. 27 (1998) 849-856.
5. K.N.C Bray, Proc. R. Soc. Lond. A431 (1990) 315-335.
6. D. Bradley, Combust. Theory and Modelling 6 (2002) 361-382.
7. L.G. Shepherd, R.K. Cheng, Combust Flame 127 (2001) 2066-2075.

8. Meng Zhang, Jinhua Wang, Wu Jin, Zuohua Huang, Hideaki Kobayashi, Lin Ma, *Combust. Flame* 162 (2015) 2087-2997.
9. E.R. Hawkes, J.H.Chen, *Combust. Flame* 144 (2006) 112-125.
10. T.D. Dunstan, N. Swaminathan, K.N.C. Bray, *J. Fluid Mech.* 709 (2012) 191-222.
11. G. Damköhler, *G. Jahrb, deut. Luftfahrtforsch, Z. Electrochem* 46 (601) (1940) 113.
12. A.N. Lipatnikov, J. Chomiak, *Progr. Energy Combust. Sci.*, 28 (2002) 1-74.
13. D. Bradley, P.H. Gaskell, X.J. Gu, A. Sedaghat, *Combust. Flame* 143 (2005) 227-245.
14. J.F. Driscoll, *Progr. Energy Combust. Sci.*, 34 (2008) 91-134.
15. J.H. Chen, H.G. Im, *Proc. Combust. Inst.* 27 (1998) 819-826.
16. J.M. Donbar, J.F. Driscoll, C.D. Carter, *Combust. Flame* 125 (2001) 1239-1257.
17. D. Bradley M. Lawes, K. Liu, M.S. Mansour, *Proc. Combust. Inst.* 34 (2013) 1519–1526.
18. D. Bradley, M. Lawes, M.S. Mansour, *Combust. Flame* 158 (2011) 123-138.
19. D. Bradley, P.H. Gaskell, X.J. Gu, *Proc. Combust. Inst* 27 (1998) 849-856.
20. A. Bagdanavicius, P.J. Bowen, N. Syred, P. Kay, A. Crayford, J. Wood, G. Sims, *AIAA Journal* 48(2) (2010) 48(2), pp 317-329, DOI 10.2514/1.43225.
21. A. Bagdanavicius, P.J.Bowen, N. Syred, A. Crayford, *Combust. Sci. Technol.* 185 (2013) 350-361.
22. A.N. Lipatnikov, J. Chomiak, *Combust. Flame* 137 (2004) 261-263.
23. X.J. Gu, M.Z. Haq, M. Lawes, R. Woolley, *Combust. Flame* 121 (2000) 41–58.
24. M. Fairweather, M.P. Ormsby, C.G.W. Sheppard, R. Woolley, *Combust. Flame* 156 (2009) 780–790.
25. D. Bradley, M. Lawes, Kexin Liu, S. Verhelst, R. Woolley, *Combust. Flame* 149 (2007) 162–172.
26. D. Bradley, R.A. Hicks, M. Lawes, C.G.W. Sheppard, R. Woolley, *Combust. Flame* 115 (1998) 126– 144.
27. T. Lachaux, F. Halter, C. Chauveu, I. Gökalp, I.G. Shepherd, *Proc. Combust. Inst.* 30 (2005) 819-826.
28. D. Bradley, M. Lawes, M.S. Mansour, *Proc. Combust. Inst.* 32 (2009) 1587-1593.
29. D. Bradley, M., Lawes, M.S Mansour, *Proc. Combust. Inst.* 33 (2011) 1269–1275.
30. J.H. Chen, H.G. Im, *Proc. Combust. Inst.* 28 (2000) 211- 218.
31. Gwang G. Lee, Kang Y. Huh, H. Kobayashi, *Combust. Flame* 122 (2000) 43–57.
32. K.N.C. Bray, N. Swaminathan, C.R. Mecanique, 334 (2006) 466-473.
33. D. Bradley, M. Lawes, M.S. Mansour, *Flow Turbulence Combust.* 87 (2011) 191-204.
34. O.L. Gülder, G.T. Smallwood, *Combust. Sci. Tech.* 179 (2007) 191–206.

35. I.G. Shepherd, R.K. Cheng, T. Plessing, C. Kortschik, N. Peters, Proc. Combust. Inst. 29 (2002) 1833–1840.
36. B.M. Deschamps, G.J. Smallwood, J. Prieur, d. R. Snelling, O . L. Gulder, Proc. Combust. Inst. 26 (1996) 427–435.
37. D. Veynante, J. M. Duclos, J. Piana, Proc, Combust. Inst. 25 (1995) 1249–1256.

Table 1. Ranges of experimental parameters in present study.

Method	Fuel	ϕ	P (MPa)	T (K)	u' (m/s)	Ma _{sr}	u_l
Burner	CH ₄	0.75,0.84, 1.1,1.2	0.3,0.7	475,575	0.78,0.83,0.9,1.07,1.16	[23]	[23]
	15% H ₂ -85% CH ₄	0.8,0.86,1.0,1 .06,1.2	0.3,0.7	475,575, 675	0.76,0.87,1.08,1.15,1.22 ,1.45,1.55,2.07	[24]	[24]
	30% H ₂ -70% CH ₄	0.83,0.9,1.03, 1.2,1.25	0.3,0.7	475,575, 675	0.87,1.01,1.08,1.16,1.23 ,1.36,1.6,1.75,1.97,2.03, 2.11,2.2,2.67	[24]	[24]
Bomb	H ₂	0.3,0.4,0.5, 0.6,0.8	0.5,0.7,1.0	358	1,2,3,4	[25]	[25]
	CH ₄	0.9	0.1,0.5,0.75 ,1.0,1.25	358	0.2,0.25,0.5,0.75,1,1.5,2	[23]	[23]
	C ₇ H ₈	1.0,1.2	0.5,0.75,1.0	358	1,2,3,4	[17]	[17]
	C ₈ H ₁₈	1.0,1.4	0.5,1.0	358	1,2,3	[26]	[26]
	10% H ₂ -90% CH ₄	0.8, 1.0,1.2	0.5,0.75,1.0	358	1,2	[17]	[23]

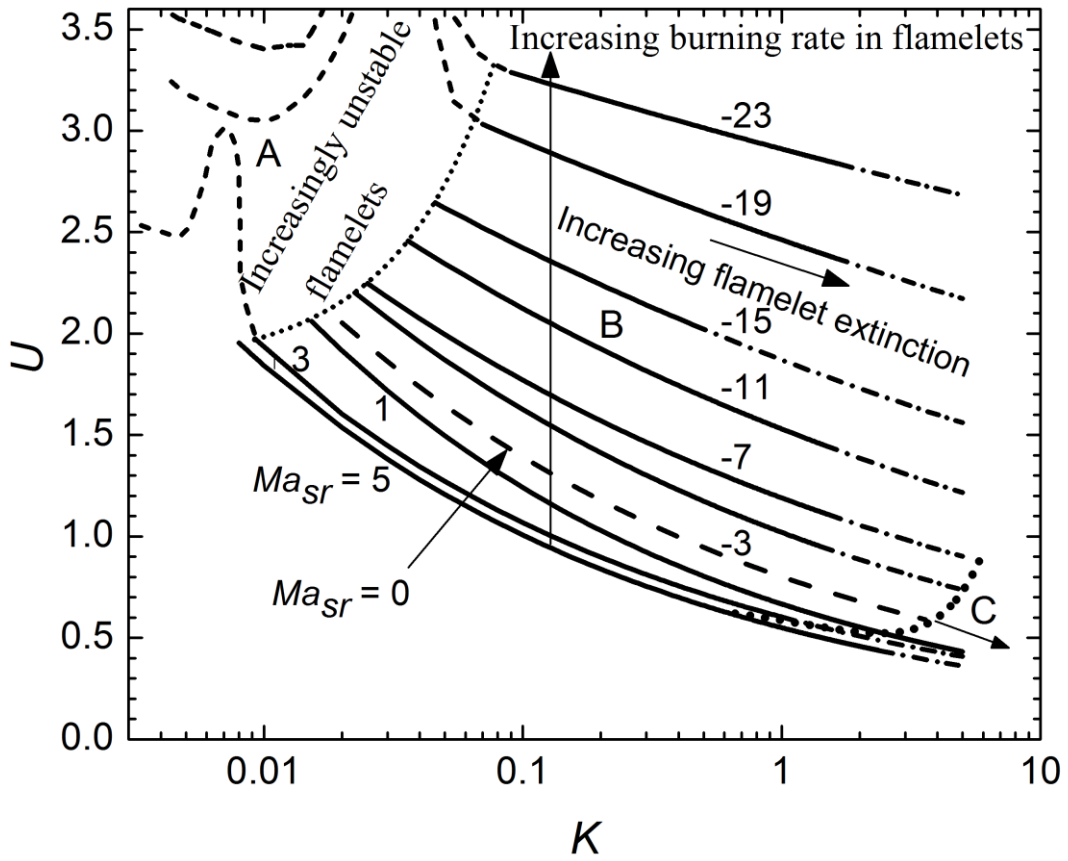


Figure 1. Regimes of turbulent combustion, showing extension of zone of unstable flamelets at increasing K as Ma_{sr} is reduced.

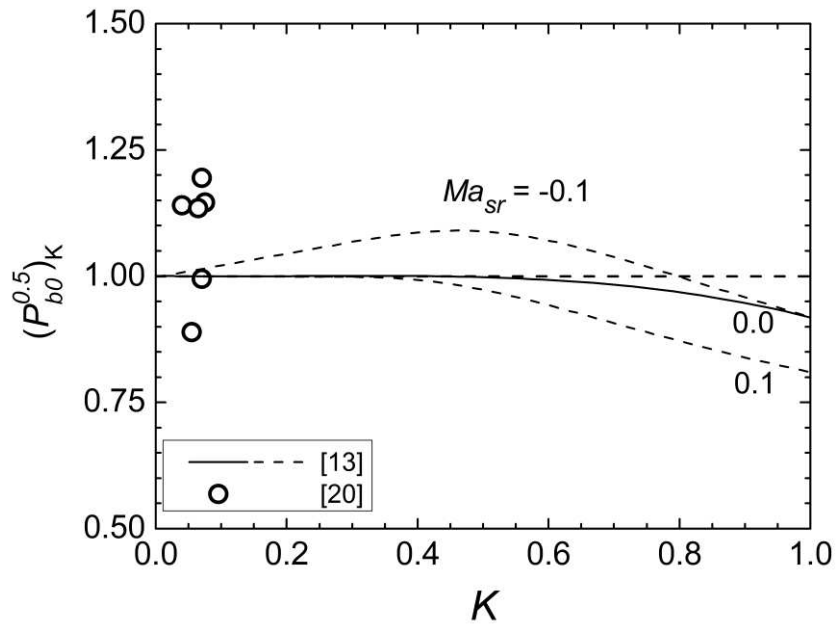


Figure 2. Dependency of $(P_b^{0.5})_K$ upon K at $Ma_{sr} \approx 0.0$. Lines indicate theoretical sensitivity of $(P_b^{0.5})_K$ to Ma_{sr} [13]. Open circle symbols derived experimentally from [20].

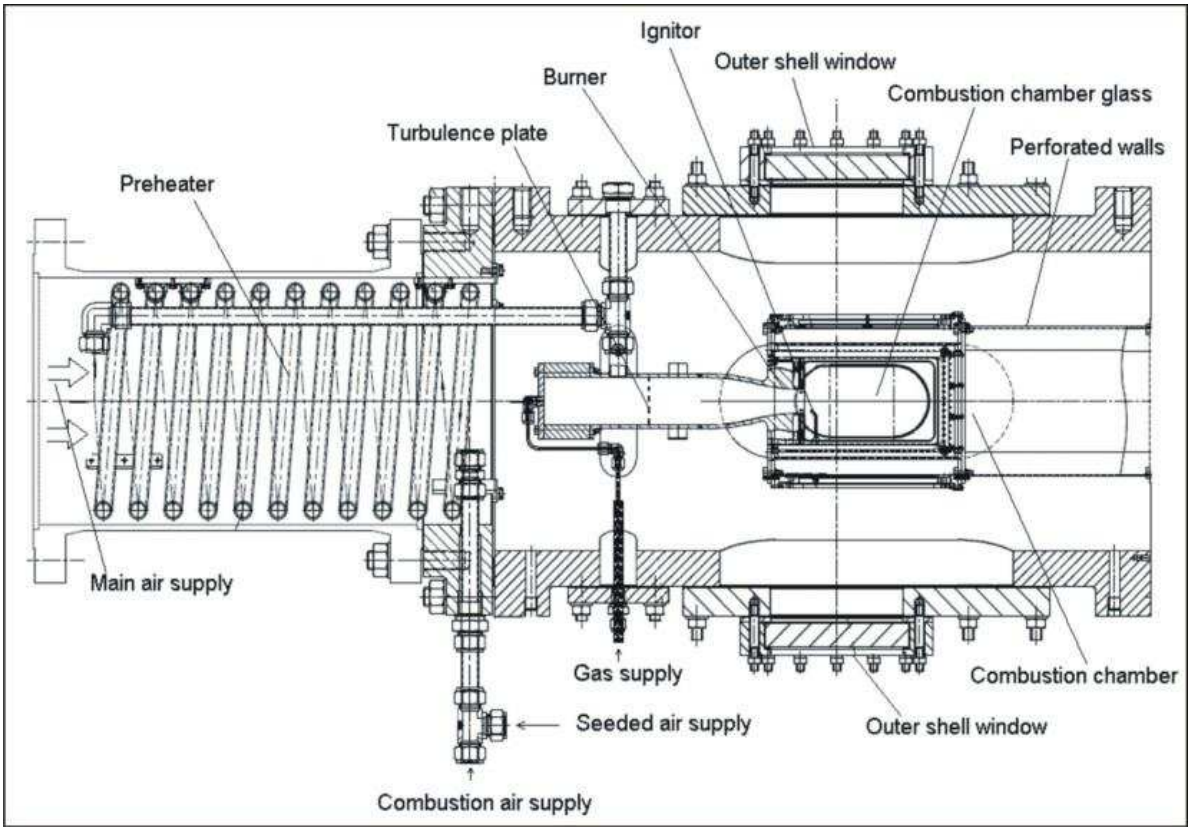


Figure 3. Cardiff High Pressure Burner.

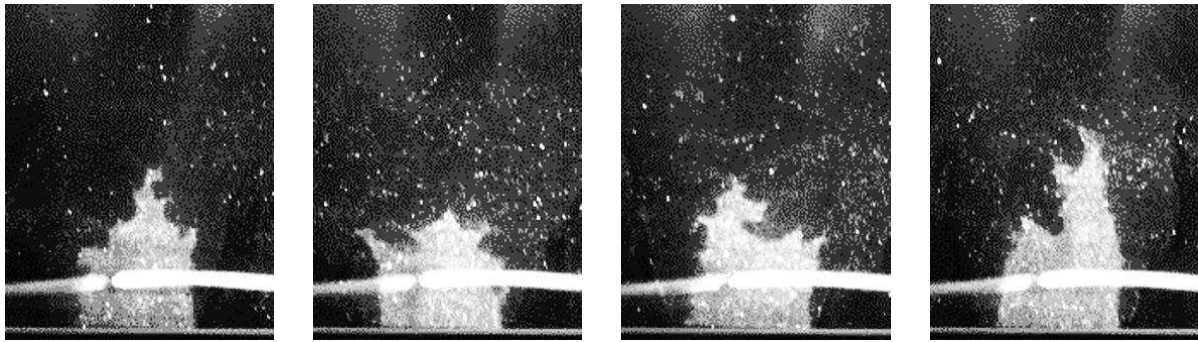


Figure 4. Mie flame images, 85% CH₄ – 15% H₂ mixture, $\phi = 1.0$, P = 0.3 MPa, T = 475K, $u' = 0.87$ m/s. (The horizontal white line in the image is the reflection from the ignition electrodes)

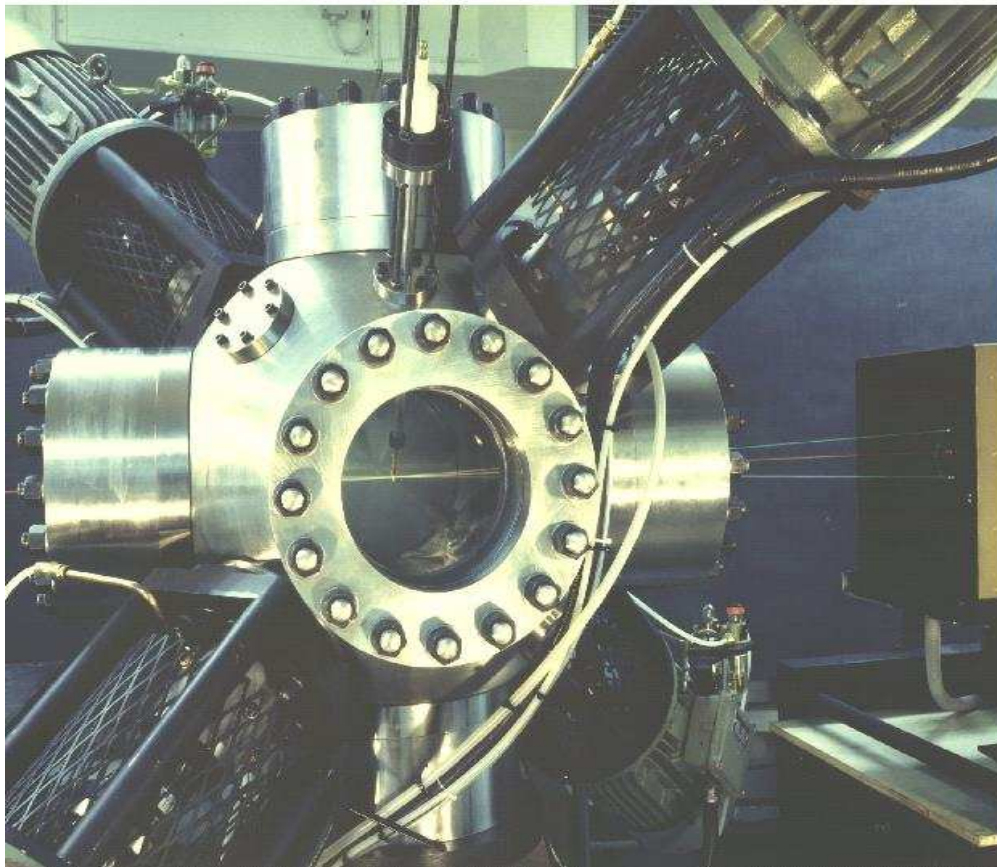


Figure 5. Leeds fan-stirred bomb.

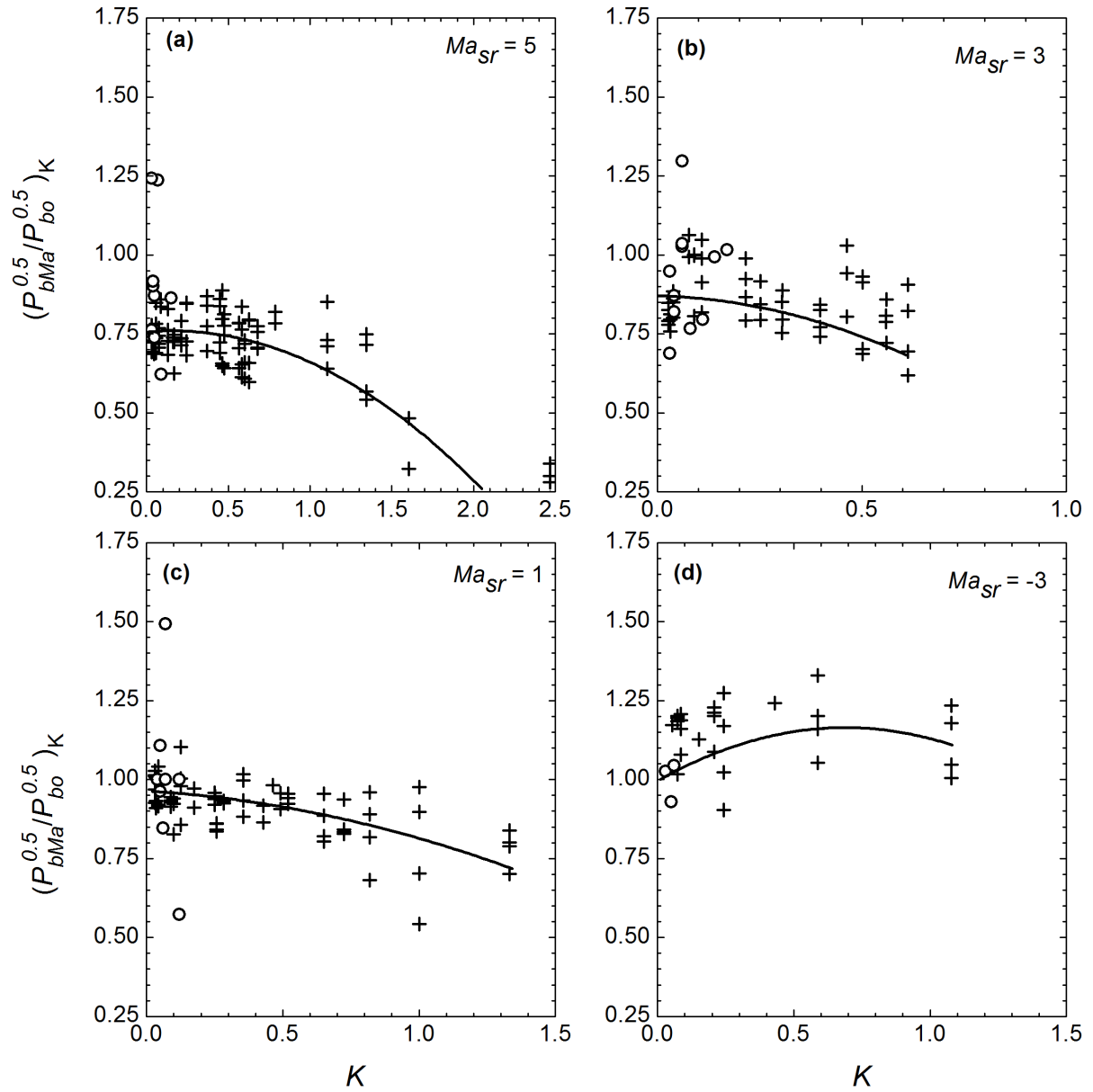


Figure 6. Variations of $(P_{bMa}^{0.5}/P_{bo}^{0.5})_K$ from Eq. (6) at different Ma_{sr} , with K for positive values of Ma_{sr} in (a), (b) and (c) and a negative value in (d). Cross symbols, derived from explosions [17,18,29], open circle symbols, derived from burner [20].

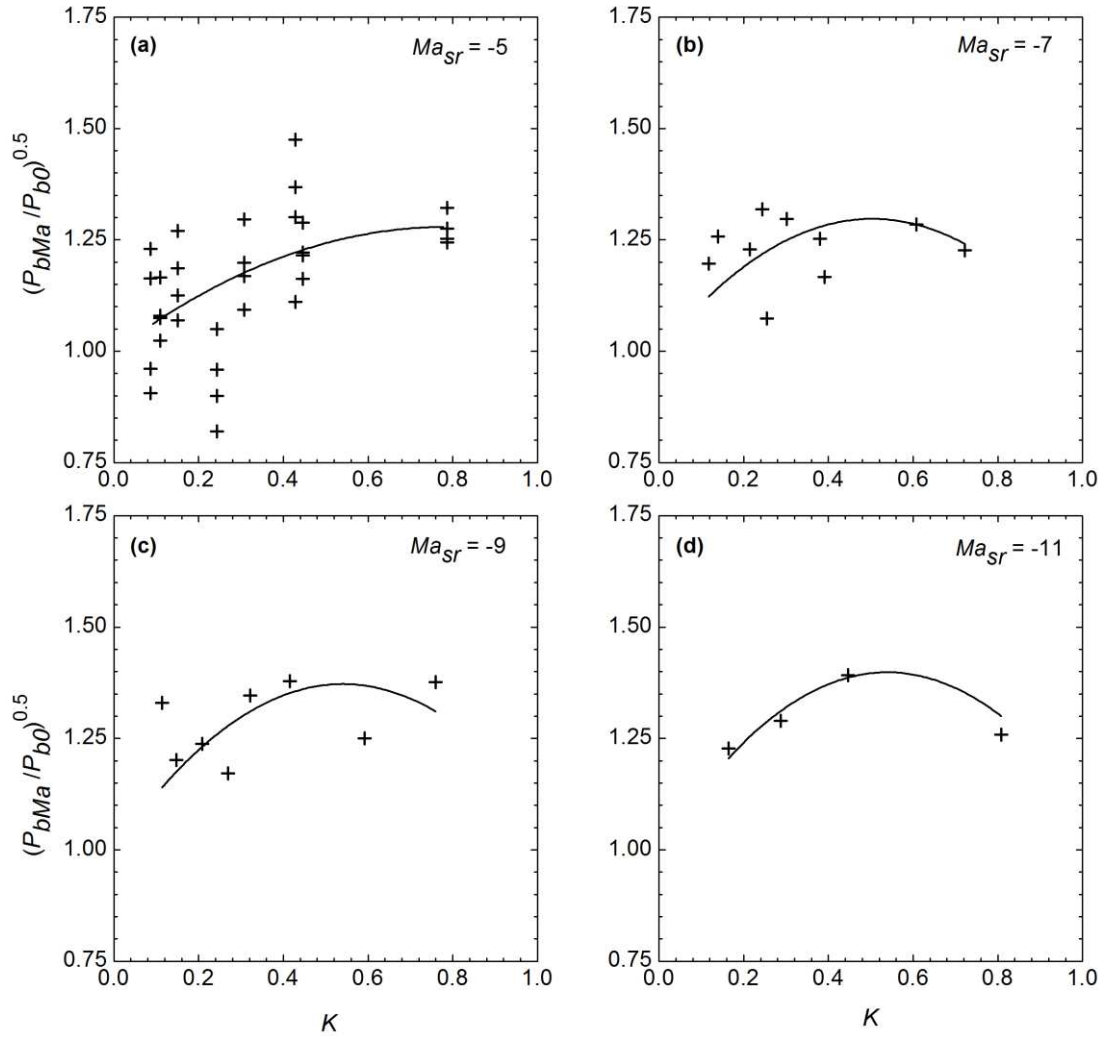


Figure 7. Variations, of $(P_{bMa}^{0.5}/P_{bo}^{0.5})_K$ from Eq. (6) at different Ma_{sr} , with K for negative values of Ma_{sr} . Cross symbols derived from [17,18,29].

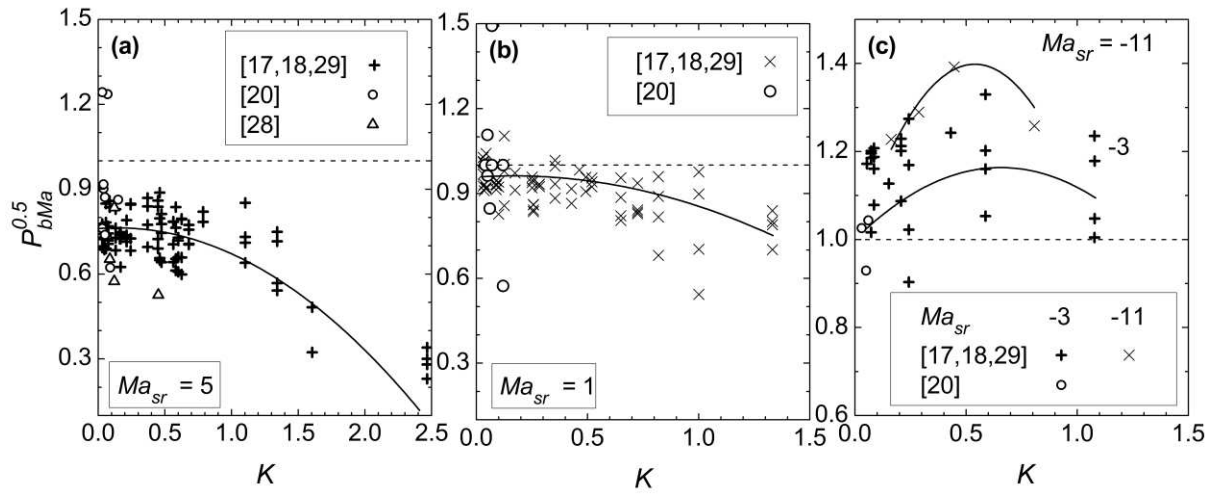


Figure 8. Some plots of $P_{bMa}^{0.5}$ derived from those $P_{bMa}^{0.5}/P_{bo}^{0.5}$ in Figs. 5 and 6, using values of $P_{bo}^{0.5}$ for $Ma_{sr} = 0$ full line curve in Fig. 2.

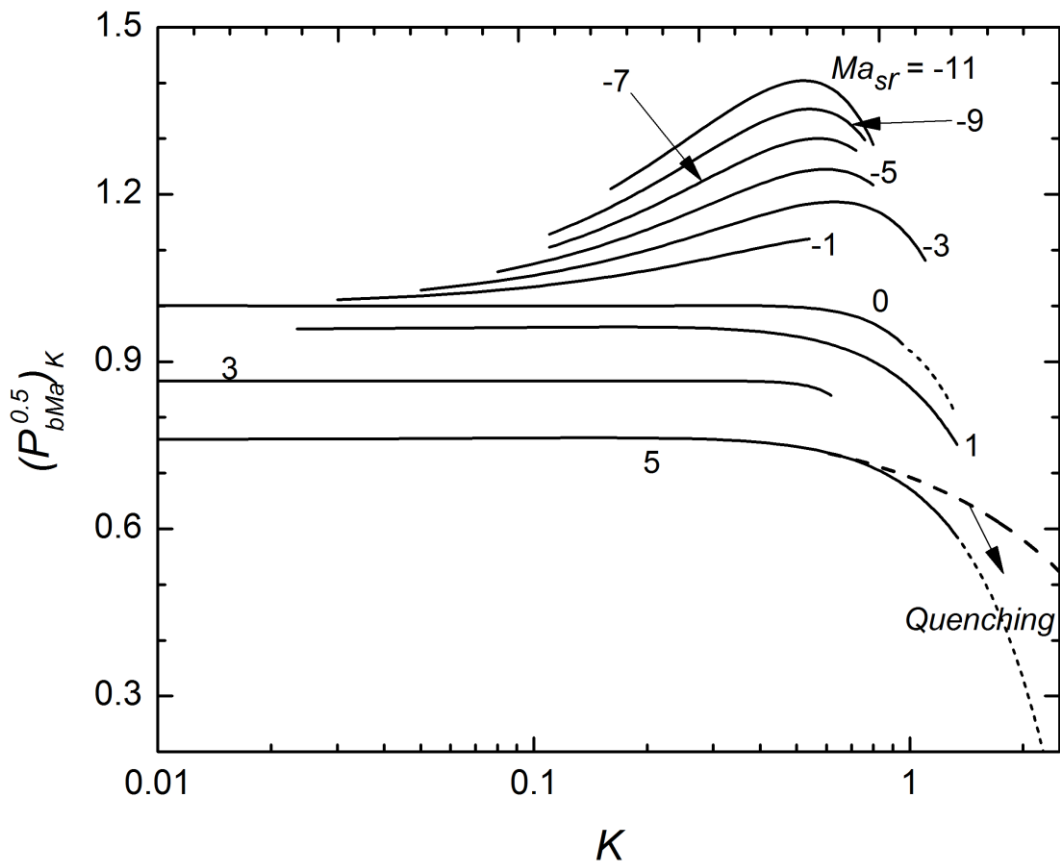


Figure 9. Correlation of $(P_{bMa}^{0.5})_K$ with K for different values of Ma_{sr} . Bold dotted curve shows approximate indication of onset of flame extinction for positive Ma_{sr} .

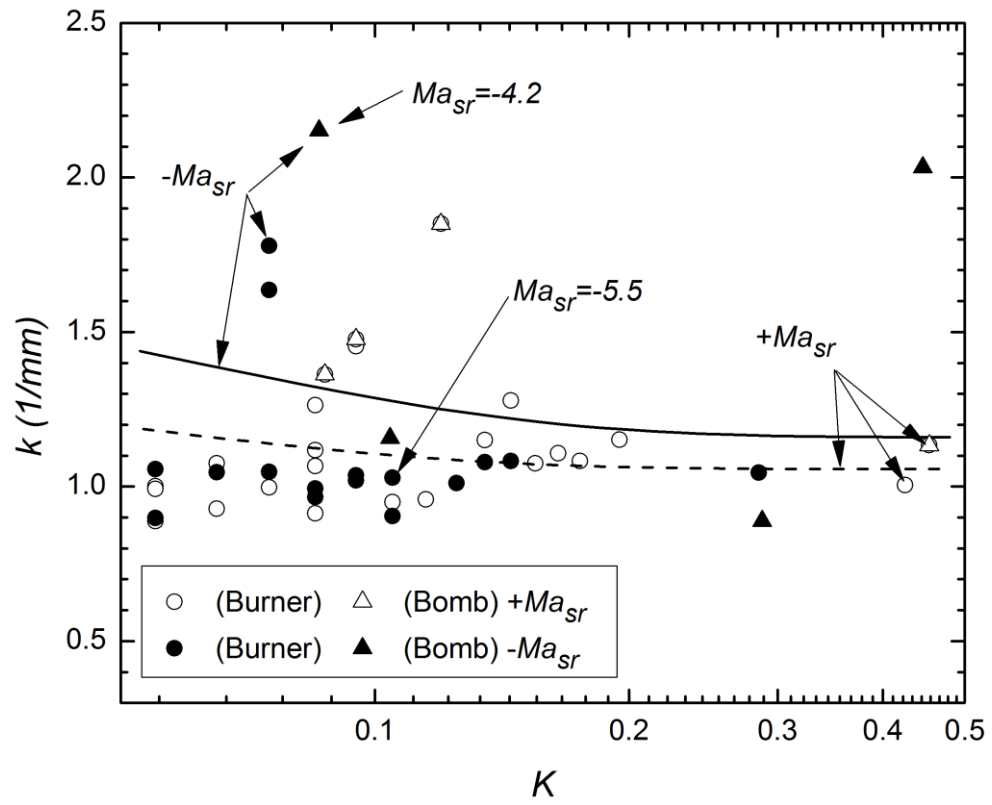


Figure 10. Correlation of k with K in present study.

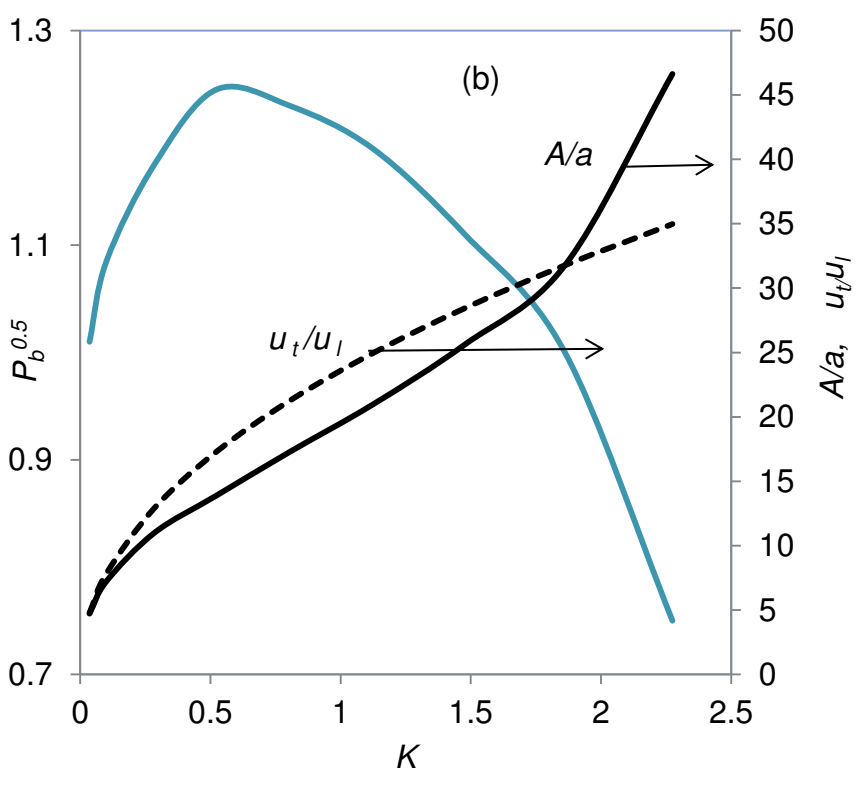
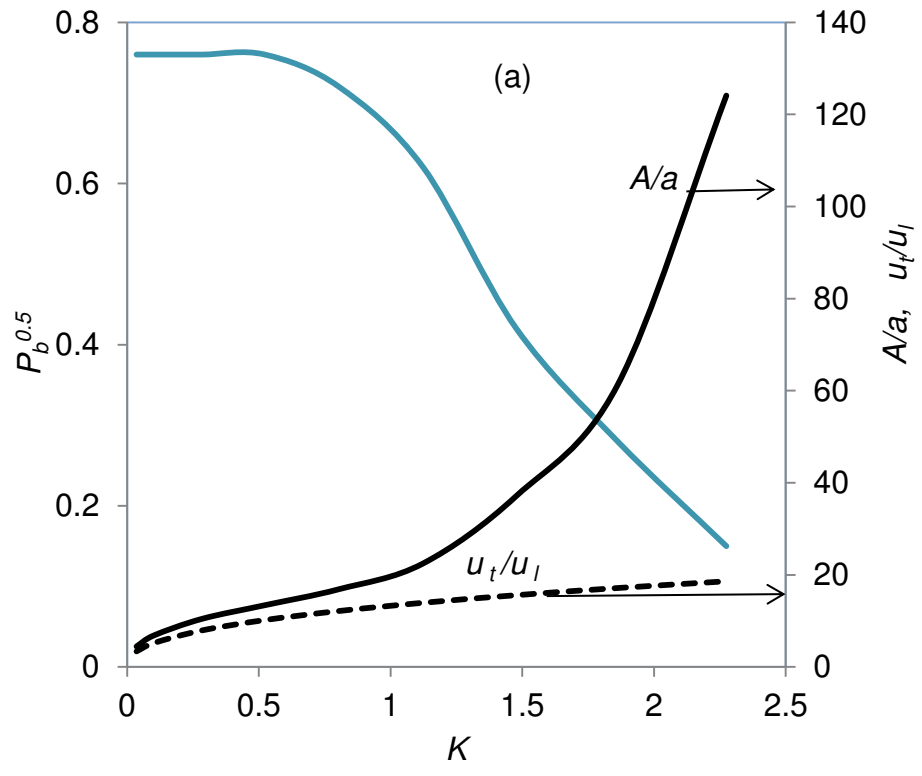


Figure 11. Effects of increasing K on $P_b^{0.5}$, A/a , and u_t/u_l , (a), for $Ma_{sr} = 5$, and (b) for $Ma_{sr} = -5$. $u_l/\nu = 27.8$.

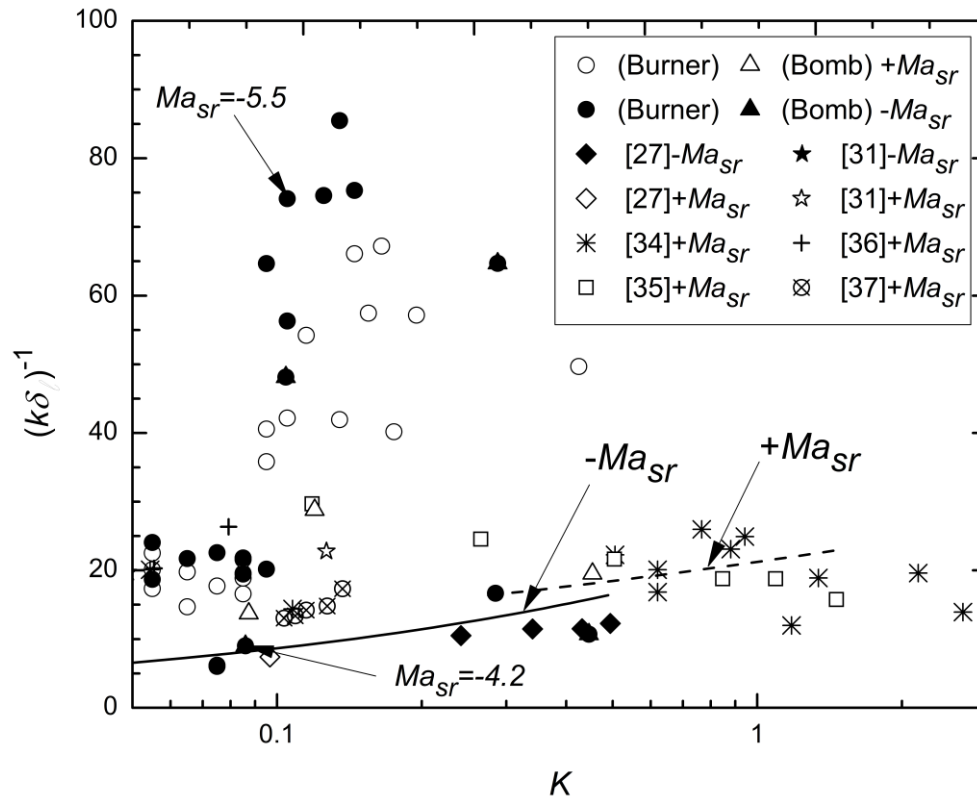


Figure 12. Correlation of the normalised wave length $(k\delta)^{-1}$ with K in present and other studies.

Figure Captions

Figure 1. Regimes of turbulent combustion, showing extension of zone of unstable flamelets at increasing K as Ma_{sr} is reduced.

Figure 2. Dependency of $(P_{bo}^{0.5})_K$ upon K at $Ma_{sr} \approx 0.0$. Lines indicate theoretical sensitivity of $(P_b^{0.5})_K$ to Ma_{sr} [13]. Open circle symbols derived experimentally from [20].

Figure 3. Cardiff High Pressure Burner.

Figure 4. Mie flame images, 85% CH_4 – 15% H_2 mixture, $\phi = 1.0$, $P = 0.3$ MPa, $T = 475$ K, $u' = 0.87$ m/s. (The horizontal white line in the image is the reflection from the ignition electrodes).

Figure 5. Leeds fan-stirred bomb.

Figure 6. Variations of $(P_{bMa}^{0.5}/P_{bo}^{0.5})_K$ from Eq. (6) at different Ma_{sr} , with K for positive values of Ma_{sr} in (a), (b) and (c) and a negative value in (d). Cross symbols, derived from explosions [17,18,29], open circle symbols, derived from burner [20].

Figure 7. Variations, of $(P_{bMa}^{0.5}/P_{bo}^{0.5})_K$ from Eq. (6) at different Ma_{sr} , with K for negative values of Ma_{sr} . Cross symbols derived from [17,18,29].

Figure 8. Some plots of $P_{bMa}^{0.5}$ derived from those $P_{bMa}^{0.5}/P_{bo}^{0.5}$ in Figs. 5 and 6, using values of $P_{bo}^{0.5}$ for $Ma_{sr} = 0$ full line curve in Fig. 2.

Figure 9. Correlation of $(P_{bMa}^{0.5})_K$ with K for different values of Ma_{sr} . Bold dotted curve shows approximate indication of onset of flame extinction for positive Ma_{sr} .

Figure 10. Correlation of k with K in present study.

Figure 11. Effects of increasing K on $P_b^{0.5}$, A/a , and u_t/u_l , (a), for $Ma_{sr} = 5$, and (b) for $Ma_{sr} = -5$. $u_l l / \nu = 27.8$.

Figure 12. Correlation of the normalised wave length $(k\delta)^{-1}$ with K in present and other studies.